Atmospheric Chemistry of Isopropyl Formate and *tert*-Butyl Formate

ANDRE SILVA PIMENTEL,[1] GEOFFREY S. TYNDALL,[2] JOHN J. ORLANDO,[2] MICHALE D. HURLEY,[3] TIMOTHY J. WALLINGTON,[3] MADS P. SULBAEK ANDERSEN,[4] PAUL MARSHALL,[5] THEODORE S. DIBBLE[6]

[1]*Departamento de Química, Pontificia Universidade Católica do Rio de Janeiro, Gávea* 22453-900, *Rio de Janeiro*, RJ, *Brazil*
[2]*National Center for Atmospheric Research*, P. O. *Box* 3000, *Boulder*, CO 80307
[3]*Physical & Environmental Sciences Department, Ford Motor Company, Mail Drop* SRL-3083, *Dearborn*, MI 48121
[4]*Department of Chemistry, University of California, Irvine, Irvine*, CA 92697
[5]*Center for Advanced Scientific Computing and Modeling, Department of Chemistry, University of North Texas,* 1155 *Union Circle*, #305070, *Denton*, TX 76203-5017
[6]*Chemistry Department, State University of New York–Environmental Science and Forestry, Syracuse*, NY 13210

Received 21 August 2009; revised 28 January 2010; accepted 3 March 2010

DOI 10.1002/kin.20498
Published online in Wiley InterScience (www.interscience.wiley.com).

ABSTRACT: Formates are produced in the atmosphere as a result of the oxidation of a number of species, notably dialkyl ethers and vinyl ethers. This work describes experiments to define the oxidation mechanisms of isopropyl formate, $HC(O)OCH(CH_3)_2$, and *tert*-butyl formate, $HC(O)OC(CH_3)_3$. Product distributions are reported from both Cl- and OH-initiated oxidation, and reaction mechanisms are proposed to account for the observed products. The proposed mechanisms include examples of the α-ester rearrangement reaction, novel isomerization pathways, and chemically activated intermediates. The atmospheric oxidation of isopropyl formate by OH radicals gives the following products (molar yields): acetic formic anhydride (43%), acetone (43%), and HCOOH (15–20%). The OH radical initiated oxidation of *tert*-butyl formate gives acetone, formaldehyde, and CO_2 as major products. IR absorption cross sections were derived for two acylperoxy nitrates derived from the title compounds. Rate coefficients are derived for the kinetics of the reactions of isopropyl formate with OH $(2.4 \pm 0.6) \times 10^{-12}$, and with Cl $(1.75 \pm 0.35) \times 10^{-11}$, and for *tert*-butyl formate with Cl $(1.45 \pm 0.30) \times 10^{-11}$ cm^3 molecule^{-1} s^{-1}. Simple group additivity rules fail to explain the observed distribution of sites of H-atom abstraction for simple formates. © 2010 Wiley Periodicals, Inc. Int J Chem Kinet 42: 479–498, 2010

INTRODUCTION

Esters are oxygenated compounds that have recently been detected in the atmosphere [1]. They are used extensively as solvents and to provide the flavors and scents in certain household goods. Esters are formed in the atmospheric oxidation of ethers. For example, tertiary butyl formate (TBF) is produced in the oxidation of methyl tertiary butyl ether (MTBE) [2–4].

$$CH_3OC(CH_3)_3 + OH \rightarrow H_2O + {}^{\bullet}CH_2OC(CH_3)_3 \quad (1)$$

$${}^{\bullet}CH_2OC(CH_3)_3 + O_2 \rightarrow O_2CH_2OC(CH_3)_3 \quad (2)$$

Correspondence to: G. S. Tyndall; e-mail: tyndall@ucar.edu.
Figures S1–S3 are available as Supporting Information in the online issue at www.interscience.wiley.com.

$$O_2CH_2OC(CH_3)_3 + NO \rightarrow NO_2 + {}^{\bullet}OCH_2OC(CH_3)_3 \quad (3)$$

$${}^{\bullet}OCH_2OC(CH_3)_3 + O_2 \rightarrow HC(O)OC(CH_3)_3 + HO_2 \quad (4)$$

MTBE has been used as a fuel additive to increase the oxygen content of fuel and hence reduce CO emissions. Although the use of MTBE has largely been discontinued in the United States, due to concerns about it contaminating ground water, it is still used in some other countries [5]. Thus, *tert*-butyl formate is a potentially important atmospheric chemical, particularly in areas where MTBE is still used [6]. It can also be formed from the atmospheric oxidation of ethyl tertiary butyl ether, which is replacing MTBE as a fuel additive, particularly in Europe.

The oxidation of vinyl ethers also leads to the formation of alkyl formates [7,8].

$$OH + CH_2{=}CH\text{-}OR \rightarrow HOCH_2\text{-}C^{\bullet}H(OR) \quad (5)$$

$$HOCH_2\text{-}C^{\bullet}H(OR) + O_2 \rightarrow HOCH_2\text{-}CH(OR)O_2 \quad (6)$$

$$HOCH_2\text{-}CH(OR)O_2 + NO \rightarrow HOCH_2\text{-}CH(OR)O^{\bullet} + NO_2 \quad (7)$$

$$HOCH_2\text{-}CH(OR)O^{\bullet} \rightarrow {}^{\bullet}CH_2OH + HC(O)OR \quad (8)$$

With the increased usage of ethers as oxygenated fuel additives in both gasoline and diesel engines [9], understanding the oxidation chemistry of esters takes on added importance. The esters studied in the current work can also be regarded as prototypes for larger, more complicated molecules formed from biofuels.

In addition to being environmentally important, esters are also of theoretical interest since the oxy radicals formed from them undergo a unique reaction, known as the alpha-ester rearrangement (where R and R′ represent either a H-atom or an alkyl group).

$$RC(O)O\text{-}CHR'O^{\bullet} \rightarrow RC(O)OH + R'C\,{}^{\bullet}O \quad (9)$$

This reaction was discovered by Tuazon et al. while studying the oxidation of ethyl acetate [10] and has since been shown to occur in a number of compounds that lead to a radical of the form $RC(O)O\text{-}CHR'O^{\bullet}$ [11–16]. The reaction involves transfer of a hydrogen atom from the carbon carrying the oxy radical to the oxygen of the carbonyl group [17,18]. The reaction appears to be accelerated by increasing substitution in either the acyl group RC(O) or the alkyl group R′, as a result of a reduced activation energy [19].

This work is part of a series of collaborative papers to investigate the mechanisms and thermochemistry of ester oxidation [11,13,16,19]. We report here experiments designed to study the chemistry of TBF, and the structurally related compound isopropyl formate (IPF). Rate coefficients are reported for the reactions of these two formates with chlorine atoms and for OH radicals with IPF; the product distributions from reaction with Cl atoms in the absence of O_2 are described, from which the initial site of attack could be deduced; product studies in the presence of NO_2 are used to identify the presence of peroxynitrate species; product distributions are reported for the Cl-atom-initiated oxidation in mixtures containing O_2, NO, and N_2, from which the behavior of the individual alkoxy radicals can be deduced. The atmospherically important reactions of IPF and TBF with OH radicals were also studied, and the branching ratios for OH attack were inferred from the observed product distributions. Theoretical quantum chemical calculations provided insight regarding the reaction mechanisms.

EXPERIMENTAL

Experiments were performed both at the National Center for Atmospheric Research (NCAR) and at the Research and Innovation Center of the Ford Motor Company. The experiments at NCAR were carried out in a cylindrical stainless steel chamber with a volume of ∼47 L [13,20]. The chamber was interfaced to a Bomem DA3.01 Fourier transform infrared (FTIR) spectrometer. Internal multipass optics inside the chamber allowed an optical path length of 32 m for analysis of reactants and products. Photolysis was initiated using a filtered Xe arc lamp directed axially down the chamber through a quartz window. The experiments at Ford were carried out in a cylindrical Pyrex chamber of volume ∼127 L coupled to a Mattson Sirius FTIR spectrometer [13,21]. External blacklamps (GE F15T8-BL) provided the photolysis light for these experiments. Product yields were determined by the spectral subtraction of calibrated reference spectra recorded in each laboratory. Absorption cross sections (units of cm^2 $molecule^{-1}$) of the principal products were HCOOH, 8.5×10^{-19} at 1119 cm^{-1}; acetone, 2.5×10^{-19} at 1231 cm^{-1}; formic acetic anhydride (AFAN), 2.5×10^{-18} at 1043 cm^{-1}. The absorption spectra for HCHO, CO and CO_2 are all very structured, so absorption cross sections are not given here since they are instrument dependent.

Most of the reactions described here were initiated by reaction of chlorine atoms with the esters, in the presence of nitric oxide, oxygen, and nitrogen. Chlorine atoms were produced by the photolysis of molecular chlorine.

$$Cl_2 + h\nu \rightarrow Cl + Cl \quad (10)$$

$$Cl + RH \rightarrow HCl + R^{\bullet} \quad (11)$$

$$R^{\bullet} + O_2 \rightarrow RO_2 \quad (12)$$

$$RO_2 + NO \rightarrow RO + NO_2 \quad (13)$$

$$RO \rightarrow \text{products} \quad (14)$$

Mixtures containing typically Cl_2 (3–10) $\times$ 10^{14} molecule cm^{-3}, NO (3–6) $\times$ 10^{14} molecule cm^{-3} and either IPF or TBF (2.4–5.0) $\times$ 10^{14} molecule cm^{-3}, and O_2 (10–600 torr) made up to a total of 700 torr in nitrogen were irradiated for several periods of 2–3 min. Additional experiments were also done in the absence of NO. Infrared spectra were taken before and after each irradiation. After analysis of the spectra, product yields were obtained from plots of the amount of product formed against the amount of formate reacted. The stated uncertainties represent two standard deviations from unweighted least-squares regressions to the data.

By varying the concentration of oxygen in the chamber, information about the reaction pathway can often be gained since many alkoxy radicals react with oxygen in competition with a unimolecular reaction path, e.g.,

$$HC(O)OCH(CH_3)O^{\bullet} \rightarrow HC(O)OH + CH_3C^{\bullet}O \quad (15)$$

$$HC(O)OCH(CH_3)O^{\bullet} + O_2 \rightarrow HC(O)OC(O)CH_3 + HO_2 \quad (16)$$

Measurement of product ratios as a function of the O_2 concentration can give quantitative information on the ratios of rate coefficients for such processes.

Experiments were also conducted to investigate the reaction mechanisms of IPF and TBF with OH radicals. A comparison was made with the products obtained from the Cl-atom-initiated oxidation, which was studied more extensively. Hydroxyl radicals were generated using the photolysis of methyl (or ethyl) nitrite in the presence of O_2 and NO.

$$CH_3ONO + h\nu \rightarrow CH_3O + NO \quad (17)$$

$$CH_3O + O_2 \rightarrow HCHO + HO_2 \quad (18)$$

$$HO_2 + NO \rightarrow OH + NO_2 \quad (19)$$

The rate coefficients for the reactions of Cl atoms with IPF and TBF and for the reaction of OH with IPF were also measured as part of this work using the relative rate method.

RESULTS

Relative Rate Studies

The rate coefficients for the reactions of chlorine atoms with IPF (24) and TBF (25) were studied relative to methanol, ethyl chloride, and acetone. Chlorine atoms were produced in the presence of the ester and the reference compound in nitrogen bath gas.

$$Cl + HC(O)OCH(CH_3)_2 \rightarrow HCl + \text{products} \quad (24)$$

$$Cl + HC(O)OC(CH_3)_3 \rightarrow HCl + \text{products} \quad (25)$$

$$Cl + \text{reference} \rightarrow \text{products} \quad (26)$$

Plots of ln[formate] vs. ln[reference] were linear with intercepts that were, within experimental uncertainty, equal to zero. The slope of the plot gives the ratio of rate coefficients k_{24}/k_{26} (or analogously for k_{25}), according to Eq. (I).

$$\ln([\text{formate}]_o/[\text{formate}]_t) = k_{24}/k_{26} \ln([\text{reference}]_o/[\text{reference}]_t) \quad (I)$$

The results of the relative rate experiments are summarized in Table I.

In the case of the reaction of IPF with Cl atoms, the rate coefficient was measured relative to methanol. The slope of the plot (shown in Fig. 1) was 0.32 $\pm$ 0.03. Using the accepted value, 5.5 $\times$ 10^{-11}, for the reference rate coefficient [22] leads to $k_{24} = (1.75 \pm 0.35) \times 10^{-11}$ cm^3 $molecule^{-1}$ s^{-1}, where the uncertainty is given as $\pm$20% to encompass the statistical error in the measurement and the uncertainty in the kinetics of the reference reaction. The rate coefficient for this reaction has not been measured previously. It is intermediate between the rate of reaction for ethyl formate (0.96–1.34) $\times$ 10^{-11} [23–25] and isopropyl acetate, 2.68 $\times$ 10^{-11} cm^3 $molecule^{-1}$ s^{-1} [23], but considerably smaller than that for *n*-propyl formate (4.6–5.6) $\times$ 10^{-11} cm^3 $molecule^{-1}$ s^{-1} [23]. It should be noted that there is evidence that the rate coefficients reported by Notario et al. [23] are 20–30% too high [25]; if so, the overall reactivity of IPF and isopropyl acetate would be indistinguishable.

The rate coefficient for reaction of Cl atoms with TBF was measured relative to acetone, ethyl chloride, and methanol. The slopes of the relative rate plots were

Table I Summary of Relative Rate Measurements

Reaction	Reference Compound	Relative Rate	k_{ref} (cm^3 molecule^{-1} s^{-1})	$10^{11}k^a$ (cm^3 molecule^{-1} s^{-1})
Cl + IPF	CH_3OH	0.32 ± 0.03	5.5×10^{-11}	1.75 ± 0.35
Cl + TBF	$CH_3C(O)CH_3$	6.55 ± 0.65	2.1×10^{-12}	1.38 ± 0.14
Cl + TBF	CH_3OH	0.24 ± 0.03	5.5×10^{-11}	1.30 ± 0.16
Cl + TBF	$C_2H_5Cl^b$	1.92 ± 0.15	7.6×10^{-12}	1.47 ± 0.12
Cl + TBF	CH_3OH^b	0.29 ± 0.02	5.5×10^{-11}	1.57 ± 0.11
OH + IPF	C_2H_4	0.30 ± 0.05	7.9×10^{-12}	0.24 ± 0.04

[a] Uncertainties in Table are $1 - \sigma$ precision on each measurement. Final uncertainties are given in the text.
[b] Measurements at Ford. Otherwise at NCAR.

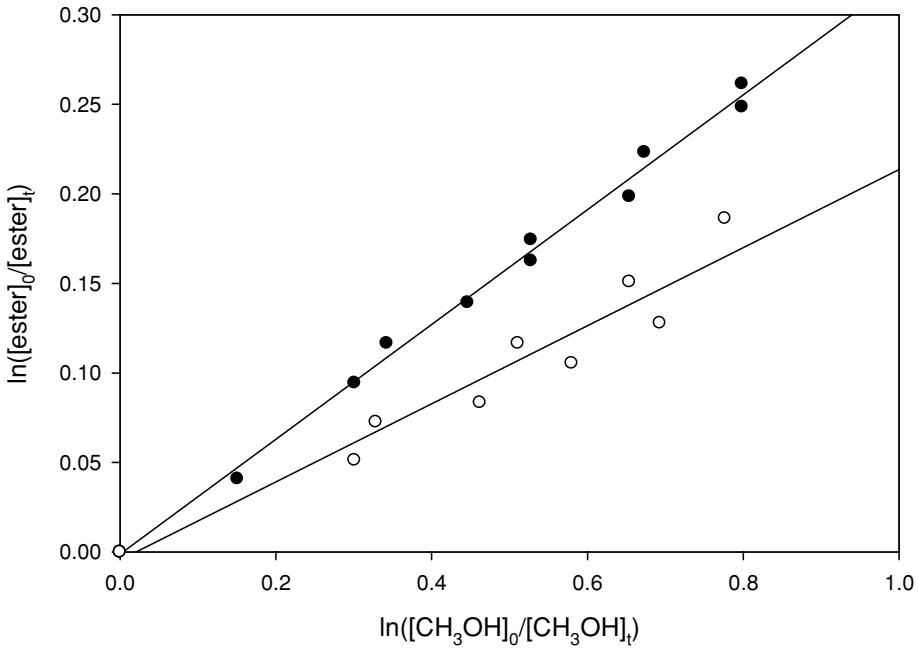

Figure 1 Plot of the relative rate equation for the reactions of chlorine atoms with IPF (●) and *tert*-butyl formate (○), using methanol as the reference compound (NCAR data).

6.55 ± 0.65 (acetone; NCAR), 0.24 ± 0.03 (methanol; NCAR), 1.92 ± 0.15 (ethyl chloride; Ford), and 0.29 ± 0.02 (methanol; Ford). Data taken relative to methanol are included in Fig. 1. Using recent values for the rate coefficients for acetone (2.1×10^{-12} [22]), ethyl chloride (7.6×10^{-12} [26]), and methanol (5.5×10^{-11} [22]) gives k_{25} (10^{-11} cm^3 molecule^{-1} s^{-1}) $= 1.38 \pm 0.14, 1.30 \pm 0.16, 1.47 \pm 0.12$, and 1.57 ± 0.11, respectively. Combining these results, we recommend $k_{25} = (1.45 \pm 0.30) \times 10^{-11}$ cm^3 molecule^{-1} s^{-1} at 298 K. The rate coefficient has never been measured before. The value obtained for k_{25} can be compared with that for *tert*-butyl acetate, 2.42×10^{-11} cm^3 molecule^{-1} s^{-1} [23]. If the results reported by Notario et al. are indeed too high, the rate coefficients for reaction of Cl atoms with *tert*-butyl formate and *tert*-butyl acetate would be indistinguishable.

It will be shown in the next section that a considerable fraction of the reaction occurs at the formate group for both IPF and TBF. It is interesting that the rate coefficients for IPF and TBF are no faster than those for the corresponding acetates, in spite of the fact that reaction at the acetyl group in the acetates is expected to be negligible [11,16].

The rate coefficient for reaction of OH with IPF was measured relative to that of ethene. The slope of the relative rate plot, shown in Fig. 2, was 0.30 ± 0.05. Combining this with the recommended value for OH + ethene at $P = 1$ atm, 7.9×10^{-12} cm^3 molecule^{-1} s^{-1} [22], leads to the value (2.4 ± 0.6) $\times 10^{-12}$ cm^3 molecule^{-1} s^{-1} at 298 K, where the uncertainty has been increased by an additional 10% to account for uncertainties in the reference reaction.

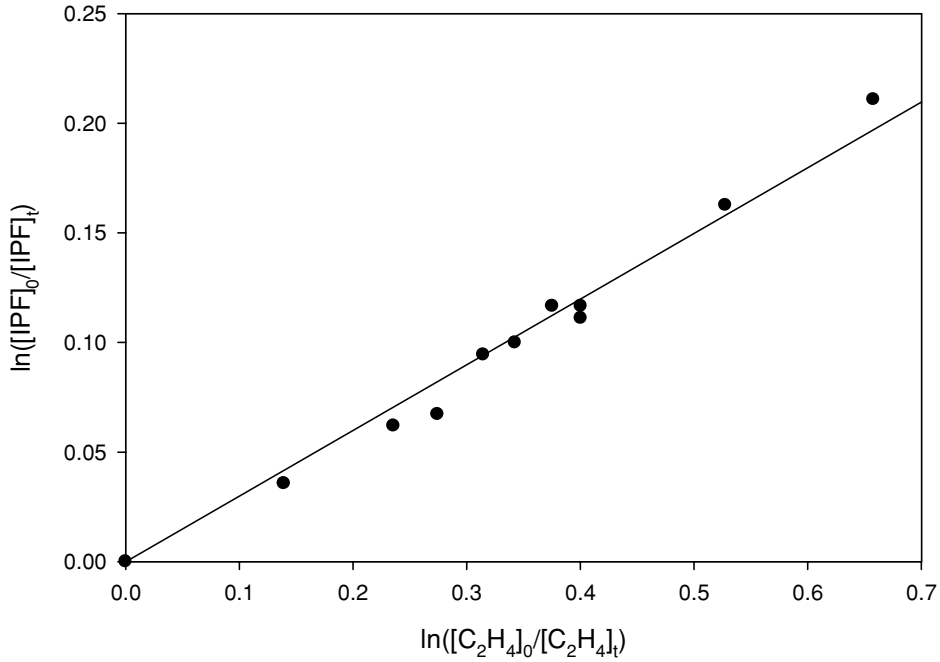

Figure 2 Plot of the relative rate equation for the reaction of OH radicals with IPF, using ethene as the reference compound.

There have been two previous determinations of this rate coefficient. Stemmler et al. [27] measured $(2.1 \pm 0.1) \times 10^{-12}$ cm^3 molecule^{-1} s^{-1} using the relative rate technique with gas chromatographic detection, and dipropyl ether as the reference compound. Szilágyi et al. [28] measured $(1.88 \pm 0.08) \times 10^{-12}$ cm^3 molecule^{-1} s^{-1} using the discharge flow technique. Our value is a little higher than both these determinations, which may reflect the uncertainty in measuring the loss of IPF accurately using FTIR.

Site of Attack

The extent of attack of Cl atoms on the formyl group of IPF and TBF was determined using the chain reaction of the ester and Cl/Cl_2 in the absence of oxygen. The systems behaved somewhat differently, as described below.

Cl + Isopropyl Formate. The UV irradiation of Cl_2–IPF–N_2 mixtures led to the appearance of a number of infrared features, including some in the characteristic C═O stretching region of acyl chlorides (1790 ± 10 cm^{-1}). By comparison with an authentic standard, significant yields were found for isopropyl chloroformate, $ClC(O)OCH(CH_3)_2$. Figure S1 in the Supporting Information shows yields of isopropyl chloroformate from the photolysis of mixtures containing $(3–34) \times 10^{14}$ molecule cm^{-3} Cl_2. The slope of the plot gives a yield of 0.30 ± 0.03, which corresponds to the fraction of attack at the formyl group in IPF. No CO or CO_2 was seen for small conversions at 296 K, indicating that the $^{\bullet}C(O)OCH(CH_3)_2$ radical does not decompose via (28) or (29).

$$Cl + HC(O)OCH(CH_3)_2 \rightarrow HCl + {}^{\bullet}C(O)OCH(CH_3)_2 \quad (24a)$$

$$^{\bullet}C(O)OCH(CH_3)_2 + Cl_2 \rightarrow ClC(O)OCH(CH_3)_2 + Cl \quad (27)$$

$$^{\bullet}C(O)OCH(CH_3)_2 \rightarrow CO_2 + {}^{\bullet}CH(CH_3)_2 \quad (28)$$

$$^{\bullet}C(O)OCH(CH_3)_2 \rightarrow CO + {}^{\bullet}OCH(CH_3)_2 \quad (29)$$

Using the rate coefficient for Cl + IPF derived above, $(1.75 \pm 0.35) \times 10^{-11}$ cm^3 molecule^{-1} s^{-1}, and a yield of isopropyl chloroformate of 30%, implies a partial rate coefficient of $(5 \pm 2) \times 10^{-12}$ cm^3 molecule^{-1} s^{-1} for reaction at the formyl group in IPF, where the error bar encompasses uncertainties in both the rate coefficient and the branching fraction. At 340 K, CO_2 was observed with a yield of ~30%, implying that thermal decomposition of the acyl radical to CO_2 + isopropyl in reaction (28) was dominant at this temperature. In the presence of larger concentrations of Cl_2 (>2×10^{15} molecule cm^{-3}) isopropyl chloroformate could be observed, indicating that the

acyloxy radicals were being trapped. No CO was observed at 340 K.

Cl + tert-Butyl Formate. Photolysis of Cl_2–TBF–N_2 mixtures with less than 6×10^{15} molecule cm^{-3} Cl_2 showed no evidence for the formation of an acyl chloride, but instead led to large yields of CO_2. The yield of CO_2 at low Cl_2 was found to be 0.50 ± 0.05 (see Fig. S2 in the Supporting Information). This presumably corresponds to the fraction of attack at the formyl group, which is followed by decomposition of the resulting *tert*-butoxycarbonyl radical.

$$Cl + HC(O)OC(CH_3)_3 \rightarrow HCl + {}^{\bullet}C(O)OC(CH_3)_3 \quad (30a)$$

$$^{\bullet}C(O)OC(CH_3)_3 \rightarrow CO_2 + {}^{\bullet}C(CH_3)_3 \quad (31)$$

Using the rate coefficient for Cl + TBF measured in this work, along with a 50% branching ratio, leads to a partial rate coefficient of $(7 \pm 2) \times 10^{-12}$ cm^3 $molecule^{-1}$ s^{-1} for attack at the formyl group, similar to that in IPF. No CO was observed from the alternative dissociation pathway.

$$^{\bullet}C(O)OC(CH_3)_3 \rightarrow CO + {}^{\bullet}OC(CH_3)_3 \quad (32)$$

On addition of larger amounts of Cl_2 ($\leq 2 \times 10^{17}$ molecule cm^{-3}) the acyl radicals were scavenged, and the CO_2 yield $Y(CO_2)$ dropped smoothly from 0.5 to 0.08.

$$^{\bullet}C(O)OC(CH_3)_3 + Cl_2 \rightarrow ClC(O)OC(CH_3)_3 + Cl \quad (33)$$

Assuming that the yield of *tert*-butyl chloroformate is given by (0.5-$Y(CO_2)$), the competition for the *tert*-butoxy carbonyl radicals can be expressed as

$$\frac{0.5 - Y(CO_2)}{Y(CO_2)} = \frac{k_{33}[Cl_2]}{k_{31}}$$

A plot of $(0.5 - Y(CO_2))/Y(CO_2)$ versus $[Cl_2]$ had a slope of $(2.8 \pm 0.7) \times 10^{-17}$ cm^3 $molecule^{-1}$. Assuming that $k_{33} > 10^{-11}$ cm^3 $molecule^{-1}$ s^{-1} [29], gives $k_{31} > 3.6 \times 10^5$ s^{-1} at 296 K. Rüegge and Fischer [30] measured the decomposition rate of $^{\bullet}C(O)OC(CH_3)_3$ radicals directly in n-heptane solution, using electron spin resonance analysis. They found $k_{31} = 6.3 \times 10^{13}$ exp (−5900/T) s^{-1}, giving a rate coefficient of 1.4×10^5 s^{-1} at 296 K.

In our previous study of chlorine atoms with methyl formate [13], the branching ratio for attack at the formyl group was 55%. However, the overall rate coefficient for Cl + methyl formate is only 1.4×10^{-12} cm^3 $molecule^{-1}$ s^{-1}, giving a partial rate coefficient at the formyl group that is an order of magnitude smaller than that measured in the present work for the Cl + TBF reaction. Thus it appears that simple group additivity cannot be used to predict the branching ratios for Cl attack on formates [23].

Product Studies in the Presence of $O_2/N_2/NO_2$

We have previously shown that the oxidation of methyl formate in the presence of NO_x leads to the production of a peroxyacyl nitrate, which is useful in identifying the extent of reaction at the acyl site [11,13]. Here we report experiments to characterize the peroxynitrates from IPF and TBF, and to obtain their IR absorption cross sections. Reaction of Cl atoms with isopropyl and *tert*-butyl formate in air in the presence of NO_2 led to the observation of numerous IR bands that could be associated with both alkylperoxy nitrates and acylperoxy nitrates. On addition of NO, bands at 1160, 1303, and 1720 cm^{-1} went away within the time it took to record a spectrum (∼4 min); these are attributed to alkyl peroxy nitrates, formed by attack at the alkyl group. Peroxyacyl nitrates derived from formates have characteristic IR absorption bands in the ranges 1230–1250 and 1820–1850 cm^{-1} [13,21,31] and are more stable than the alkyl peroxy nitrates [13].

$$Cl + HC(O)OR \rightarrow HCl + ROC^{\bullet}O \quad (21)$$

$$ROC^{\bullet}O + O_2 \rightarrow ROC(O)O_2 \quad (22)$$

$$ROC(O)O_2 + NO_2 + M \rightarrow ROC(O)O_2NO_2 + M \quad (23)$$

In this work, the alkoxyformyl peroxy nitrates $(CH_3)_2CHOC(O)O_2NO_2$ (iPOPAN) and $(CH_3)_3COC(O)O_2NO_2$ (tBOPAN) were identified as arising from the oxidation of IPF and TBF, respectively. These species decayed in the presence of NO with a lifetime of about 1 h. At the conclusion of the experiments, absorption bands attributed to nitrites and nitrates could be seen in the spectra at 1160–1170 and 1290–1300 cm^{-1}.

Upon addition of NO to the products from IPF, absorption features of AFAN, acetone and formic acid appeared rapidly. After decay of the unstable peroxynitrate(s), the residual bands (795, 910, 1109, 1233, 1745, and 1827 cm^{-1}) are assigned to the peroxyacyl nitrate $(CH_3)_2CHOC(O)O_2NO_2$ (iPOPAN). Using the

branching ratio derived earlier for reaction of Cl atoms at the formyl group (30%) leads to peak infrared absorption cross sections for iPOPAN (cm^2 $molecule^{-1}$) of $(5.2 \pm 0.8) \times 10^{-18}$ at 1233 cm^{-1}, $(3.1 \pm 0.5) \times 10^{-18}$ at 1745 cm^{-1}, and $(1.9 \pm 0.3) \times 10^{-18}$ at 1827 cm^{-1}. These cross sections are similar to those found in our previous work on the methoxy analog [13] and roughly a factor of 2 higher than the corresponding bands of peroxyacetyl nitrate (PAN) [32,33]. Formation of iPOPAN was also observed in experiments at 270 K. The absorption cross sections of PAN change by less than 10% over this temperature range [33]. Assuming that iPOPAN cross sections are also independent of temperature, a yield of 30% is obtained, demonstrating that the branching fraction for Cl-atom attack on the formyl site does not vary strongly with temperature.

Reaction of Cl atoms with TBF in the presence of NO_2 in air led to the production of an alkyl peroxy nitrate and the acyl peroxy nitrate, $(CH_3)_3COC(O)O_2NO_2$ (tBOPAN). This compound has been previously identified by Kirchner et al. [31]. Using a branching fraction of (50 ± 5)% for reaction of Cl atoms at the formyl group, absorption cross sections (cm^2 $molecule^{-1}$) of $(5.5 \pm 0.8) \times 10^{-18}$ at 1239 cm^{-1} and $(2.1 \pm 0.3) \times 10^{-18}$ at 1827 cm^{-1} were obtained for $(CH_3)_3COC(O)O_2NO_2$.

Addition of NO led to the rapid decay of the alkyl peroxy nitrate, accompanied by production of CO_2 and acetone. The tBOPAN decomposed with a 1/*e* time of around 1 h, somewhat slower than the 15-min lifetime reported by Kirchner et al. [31]. During the decay of tBOPAN, acetone was observed as a product. Figure 3 shows the products obtained during the dark decay of tBOPAN in the presence of excess NO. At the levels of NO and NO_2 present, it would be expected that *tert*-butoxy radicals would be scavenged to form *tert*-butyl nitrite or *tert*-butyl nitrate [22]. However, acetone is found in a yield of ~30% per tBOPAN decomposed (or 15% of the TBF reacted away), suggesting rapid decomposition of activated *tert*-butoxy radicals.

To compare the spectra of the peroxyacyl nitrates formed from methyl formate (MOPAN) [13], IPF (iPOPAN), and *tert*-butyl formate (tBOPAN), the infrared bands at ~1230–1240 cm^{-1} were integrated. The integrated cross sections for the three molecules were 1.1×10^{-16}, 8.0×10^{-17}, and 8.6×10^{-17} cm $molecule^{-1}$. Considering that a number of reference spectra have to be subtracted to obtain the residual absorptions, the values can be considered to be equal within the experimental uncertainties, showing consistency within the measurements of the branching fractions.

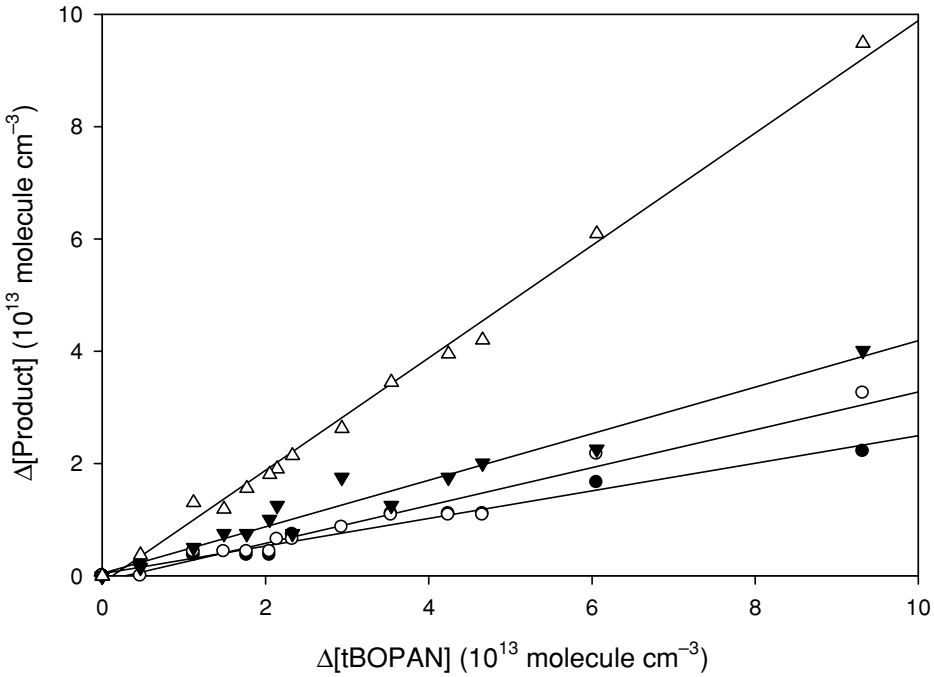

Figure 3 Product yields observed during the dark decay of tBOPAN in the presence of NO. ●, *tert*-BuONO; ○, acetone; ▼, *tert*-$BuONO_2$; □, total.

Product Studies in the Presence of $O_2/N_2/NO$

Isopropyl Formate. Reaction of Cl atoms with IPF can occur by hydrogen atom abstraction at three sites, leading to the formation of three peroxy/oxy radicals.

$$Cl + HC(O)OCH(CH_3)_2\ (+ O_2) \rightarrow HCl + O_2C(O)OCH(CH_3)_2 \quad (24a)$$

$$O_2C(O)OCH(CH_3)_2 + NO \rightarrow NO_2 + CO_2 + {}^{\bullet}OCH(CH_3)_2 \quad (35a)$$

$$Cl + HC(O)OCH(CH_3)_2\ (+ O_2) \rightarrow HCl + HC(O)OC(CH_3)_2O_2 \quad (24b)$$

$$HC(O)OC(CH_3)_2O_2 + NO \rightarrow NO_2 + HC(O)OC(CH_3)_2O^{\bullet} \quad (35b)$$

$$Cl + HC(O)OCH(CH_3)_2\ (+ O_2) \rightarrow HCl + HC(O)OCH(CH_3)CH_2O_2 \quad (24c)$$

$$HC(O)OCH(CH_3)CH_2O_2 + NO \rightarrow NO_2 + HC(O)OCH(CH_3)CH_2O^{\bullet} \quad (35c)$$

The oxidation of IPF was studied in the presence of NO at a total pressure of 700 torr, with the partial pressure of O_2 varied between 20 and 450 torr. Experiments were also conducted using mixtures containing zero NO and at 270 K. The major products observed in all experiments were HCHO, CO, CO_2, HCOOH, acetic formic anhydride (AFAN, $HC(O)OC(O)CH_3$), acetone ($CH_3C(O)CH_3$), and the acyl peroxy nitrate iPOPAN ($(CH_3)_2CHOC(O)O_2NO_2$). The major pathways in the oxidation of IPF leading to these products are summarized in the lower half of Reaction Scheme 1 later in this paper.

Representative product data in air are shown in Fig. 4, and yields of the observed products for a variety of starting conditions are given in Table II. Product yields measured at short reaction times (i.e., small extent of conversion) were not found to be strongly dependent on the O_2 partial pressure. Data from experiments at different O_2 partial pressures were combined to give yields of acetone ($30 \pm 5\%$), AFAN ($30 \pm 4\%$), formic acid ($15 \pm 5\%$), and CO_2 ($52 \pm 8\%$). The yield plots of acetone and CO_2 versus Δ(IPF) were found to curve downward at high conversion, as the iPOPAN yield increased. This was a result of competition for the acyl peroxy radical $(CH_3)_2CHOC(O)O_2$ reacting with either NO or NO_2. A plot of [acetone] + [iPOPAN] was linear with a slope of 0.38 ± 0.05. The sum of the yields of acetone, AFAN, HCOOH and iPOPAN was between 75 and 85%, accounting for most of the reacted IPF. Some of the run-to-run variability in the

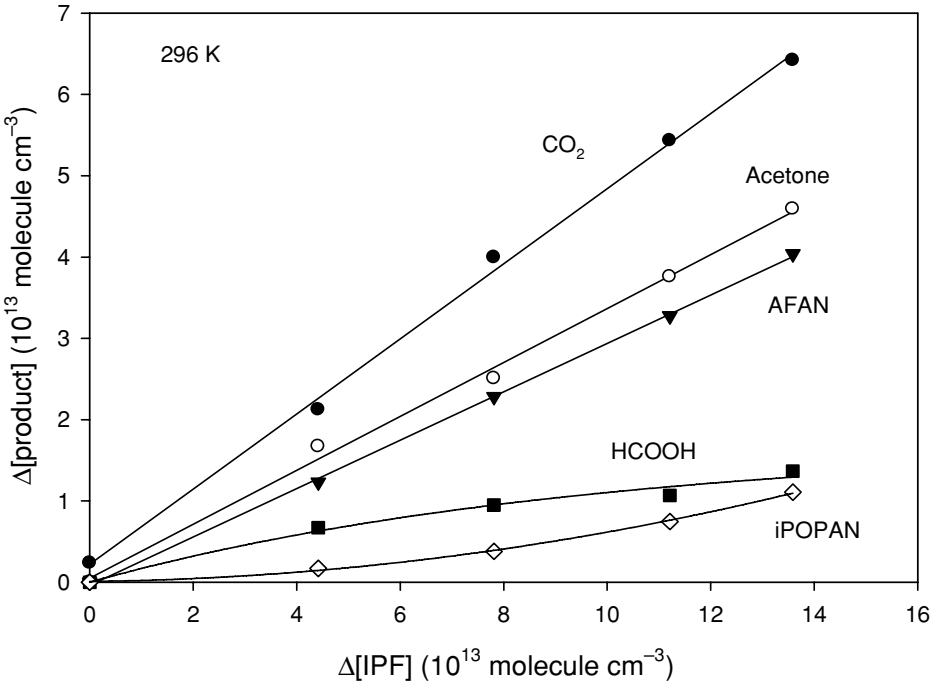

Figure 4 Formation of products from the reaction of Cl atoms with IPF in the presence of NO (5.5×10^{14} molecule cm^{-3}) and 140 torr O_2 (made up to 700 torr with N_2) at 296 K. ●, CO_2; ○, acetone; ▼, AFAN; ■, HCOOH; ◇, iPOPAN.

Table II Experimental Conditions and Product Yields for the Reaction of IPF with Cl Atoms in the Presence of NO

			Product Yields (%)						
$P(O_2)$ (torr)	[IPF]o ($\times 10^{14}$)	[NO]o ($\times 10^{14}$)	CO_2	CO_2+ iPOPAN	Acetone	Acetone + iPOPAN	AFAN	HCOOH	CO + HCHO
140	3.5	5.6	59	65	33	38	27	8	37
450	3.5	5.6	52	56	32	41	30	10	36
150	3.5	5.6	64	71	25	32	30	12	35
450	3.5	6.5	41	51	27	35	28	12	32
20	3.5	6.8	51	58	28	32	27	18	24
140	3.4	5.5	48	56	34	42	30	15	33
20	3.4	5.5	50	59	30	37	29	14	28
450	3.4	5.5	39	50	28	38	31	10	35
140[a]	3.5	5.4	37	46	45	53	16	20	10
20[a]	3.5	5.4	38	44	45	51	16	20	15
400[a]	3.5	5.2	34	44	41	51	19	19	11

[a]Expt. at 270 K.

yields is caused by differences in secondary chemistry as the ratios O_2/NO_x and NO/NO_2 varied. Interestingly, there was no obvious dependence of the acetone yield on the ratio $[O_2]/[NO]$ nor was there any strong evidence for the formation of isopropyl nitrite or nitrate. These observations will be further discussed later.

The yields of CO and HCHO were combined, since the very rapid reaction of HCHO with Cl atoms converts it to CO.

$$Cl + HCHO \rightarrow HCl + HCO \quad (36)$$

$$HCO + O_2 \rightarrow HO_2 + CO \quad (37)$$

At high $[O_2]$ the yield of CO + HCHO was 40%. At low O_2 (20 torr) methyl nitrite and methyl nitrate were also observed, indicating that part of the HCHO originated from CH_3O radicals.

$$CH_3O + O_2 \rightarrow HCHO + HO_2 \quad (18)$$

$$CH_3O + NO + M \rightarrow CH_3ONO + M \quad (38)$$

$$CH_3O + NO_2 + M \rightarrow CH_3ONO_2 + M \quad (39)$$

The variation of the sum ($CH_3ONO + CH_3ONO_2$) with O_2 concentration was consistent with the known rate coefficients for reactions (18), (38), and (39) [22] and led to a CH_3O yield of $(35 \pm 5)\%$. The total yield of (HCHO + methyl nitrate + methyl nitrite) approached 55%, implying a direct HCHO yield close to 20%. The most likely direct source of HCHO is from decomposition of the $HC(O)OCH(CH_3)CH_2O^\bullet$ radical (40); no spectral features were identified which could be attributed to 2-formoxypropanal from its reaction with O_2 (41).

$$HC(O)OCH(CH_3)CH_2O^\bullet \rightarrow HC(O)OC^\bullet H(CH_3) + HCHO \quad (40)$$

$$HC(O)OCH(CH_3)CH_2O^\bullet + O_2 \rightarrow HO_2 + HC(O)OCH(CH_3)CHO \quad (41)$$

The inferred yield of methyl radicals (~35%) was very close to that of AFAN, suggesting a common source from the $HC(O)OC(CH_3)_2O^\bullet$ radical.

$$HC(O)OC(CH_3)_2O^\bullet \rightarrow HC(O)OC(O)CH_3 + CH_3 \quad (42)$$

Oxidation at the formyl group in IPF (reaction (24a)) should lead to the isopropoxy radical, which is known to react with O_2 to produce acetone.

$$O_2C(O)OCH(CH_3)_2 + NO \rightarrow NO_2 + CO_2 + (CH_3)_2CHO^\bullet \quad (35a)$$

$$(CH_3)_2CHO^\bullet + O_2 \rightarrow HO_2 + CH_3C(O)CH_3 \quad (43)$$

However, reaction (43) cannot be the only source of acetone, since the yield of acetone plus iPOPAN exceeds 30%, which is the fraction of abstraction at the H—C(O) bond determined earlier. Furthermore, acetone was formed from decomposition of the unstable alkylperoxy nitrates (see the section Product Studies in the Presence of $O_2/N_2/NO_2$). It is proposed that decomposition of the tertiary alkoxy radical $HC(O)OC(CH_3)_2O^\bullet$ leads to the formation of either

AFAN (42) or acetone (44)–(46). Direct decomposition to give acetone and HCO_2 is also possible (47), but such C—O bond fissions are thought to have a higher barrier and are not expected to occur at 296 K [17,18,34,35].

$$HC(O)OC(CH_3)_2O^\bullet \rightarrow CH_3 + HC(O)OC(O)CH_3 \quad (42)$$

$$HC(O)OC(CH_3)_2O^\bullet \rightarrow {}^\bullet C(O)OC(CH_3)_2OH \quad (44)$$

$${}^\bullet C(O)OC(CH_3)_2OH \rightarrow CO_2 + {}^\bullet C(CH_3)_2OH \quad (45)$$

$${}^\bullet C(CH_3)_2OH + O_2 \rightarrow HO_2 + CH_3C(O)CH_3 \quad (46)$$

$$HC(O)OC(CH_3)_2O^\bullet \rightarrow HCO_2 + CH_3C(O)CH_3 \quad (47)$$

The combined yields of acetone and iPOPAN total 35–40%. Since abstraction at the formyl site accounts for only 30%, the additional acetone must come from the tertiary site. Decomposition of the $HC(O)OC(CH_3)_2O^\bullet$ radical thus produces AFAN ($30 \pm 5\%$) and acetone ($10 \pm 5\%$). The observation that acetone was formed from the decomposition of the alkyl peroxy nitrates (see the section Product Studies in the Presence of $O_2/N_2/NO_2$) is very strong evidence for the occurrence of reactions (44) and/or (47). It will be argued later that the product distribution largely results from chemical activation of the radicals, rather than a thermal distribution.

The remaining abstraction occurs at the primary methyl groups, leading to the production of formic acid through the α-ester rearrangement (15).

$$HC(O)OCH(CH_3)CH_2O_2 + NO \rightarrow NO_2 + HC(O)OCH(CH_3)CH_2O^\bullet \quad (35c)$$

$$HC(O)OCH(CH_3)CH_2O^\bullet \rightarrow HCHO + HC(O)OC^\bullet H(CH_3) \quad (40)$$

$$HC(O)OC^\bullet H(CH_3) + O_2 \rightarrow HC(O)OCH(CH_3)O_2 \quad (48)$$

$$HC(O)OCH(CH_3)O_2 + NO \rightarrow HC(O)OCH(CH_3)O^\bullet + NO_2 \quad (49)$$

$$HC(O)OCH(CH_3)O^\bullet \rightarrow HC(O)OH + CH_3C^\bullet O \quad (15)$$

The $HC(O)OCH(CH_3)O^\bullet$ radical is also formed in the oxidation of ethyl formate [19,36]. It has five available reaction pathways: reaction with O_2, elimination of $-CH_3$, C—O dissociation, isomerization through a five-membered transition state, and the alpha-ester rearrangement. Orlando and Tyndall [19] have shown that this radical reacts predominantly by the α-ester reaction at room temperature, in competition with reaction with O_2. The ratio of rate coefficients found at room temperature in that work was $k_{15}/k_{16} = 4 \times 10^{19}$ molecule cm^{-3}. Assuming a rate coefficient for reaction (16) of 1×10^{-14} cm^3 $molecule^{-1}$ s^{-1} leads to a decomposition rate of 4×10^5 s^{-1}; however, there is evidence to suspect that reactions of alkoxy radicals with O_2 that are highly exothermic such as (16) may be faster than the canonical value given above [34].

$$HC(O)OCH(CH_3)O^\bullet \rightarrow HCOOH + CH_3CO \quad (15)$$

$$HC(O)OCH(CH_3)O^\bullet + O_2 \rightarrow HC(O)OC(O)CH_3 + HO_2 \quad (16)$$

The observed yield of formic acid was 15–20% at short reaction times, consistent with the direct formaldehyde yield. The yields of HCOOH given in Table II show only a weak dependence on O_2, consistent with the large value of k_{15}/k_{16} given above. The HCOOH yield decreased as the reaction proceeded (see Fig. 4), which is probably a consequence of a precursor to formic acid being scavenged by NO_2, which builds up during the course of an experiment. The concentration of NO_2 builds up faster at higher O_2 (because of the reaction NO + NO + O_2), which could account for some of the apparent O_2 dependence. The yields of acetone + iPOPAN + AFAN + formic acid add up to ($82 \pm 15\%$), accounting for most of the reacted carbon. Some formation of large, multifunctional organic nitrates was observed, which could account for the rest of the reaction. Peroxyacetyl nitrate should also be produced from the acetyl radicals formed in reaction (15). However, its most prominent IR band, at 1164 cm^{-1}, was obscured by the multifunctional nitrates. No evidence was found for production of formic anhydride, the product of reaction (50).

$$HC(O)OCH(CH_3)O^\bullet \rightarrow HC(O)OCHO + CH_3 \quad (50)$$

As the reaction proceeds, NO is converted to NO_2. The variation of the NO/NO_2 ratio during the course of an experiment (0.3–6) allowed an estimation of the relative rate coefficients for the reactions of the acyl peroxy radical with NO and NO_2.

$$(CH_3)_2CHOC(O)O_2 + NO \rightarrow NO_2 + CO_2 + (CH_3)_2CHO^\bullet \quad (35a)$$

$$(CH_3)_2CHOC(O)O_2 + NO_2 \rightarrow (CH_3)_2CHOC(O)O_2NO_2 \quad (51)$$

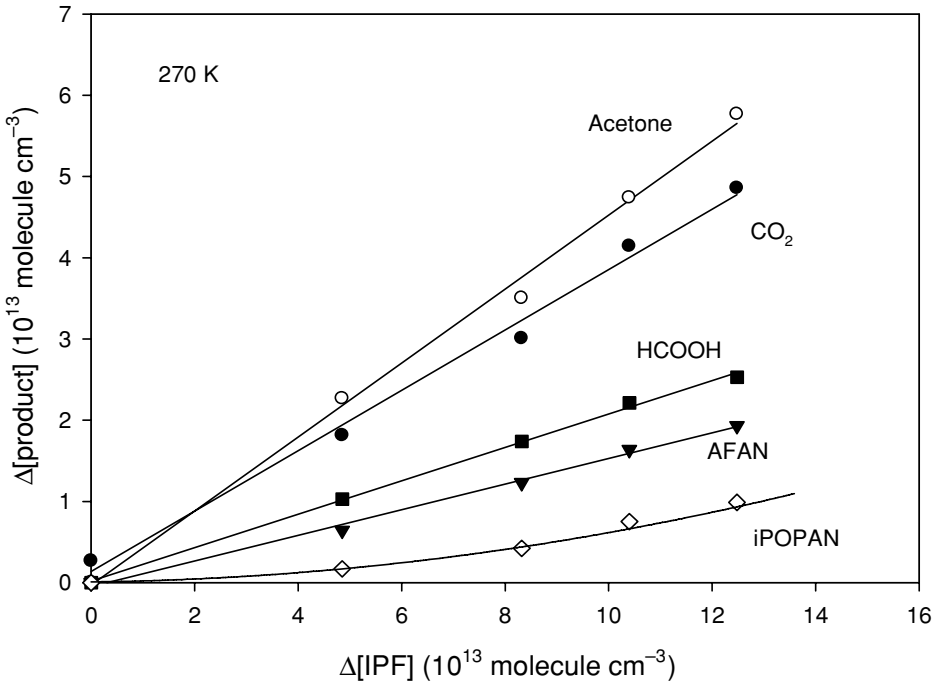

Figure 5 Formation of products from the reaction of Cl atoms with IPF in the presence of NO (5.4×10^{14} molecule cm^{-3}) and 140 torr O_2 (made up to 700 torr with N_2) at 270 K. ●, CO_2; ○, acetone; ▼, AFAN; ■, HCOOH; ◇, iPOPAN.

Thus, the yield of iPOPAN is given by

$$\mathrm{Y(iPOPAN)} = \mathrm{Y(formyl)} \times \frac{k_{51}[\mathrm{NO_2}]}{k_{51}[\mathrm{NO_2}] + k_{35a}[\mathrm{NO}]}$$

or

$$\frac{\Delta[\mathrm{IPF}]}{\Delta[\mathrm{iPOPAN}]} = \frac{1}{\mathrm{Y(formyl)}} \times \left(1 + \frac{k_{35a}[\mathrm{NO}]}{k_{51}[\mathrm{NO_2}]}\right)$$

where Y(formyl) is the fractional attack of Cl at the formyl site. The quantity 1/Y(iPOPAN) = Δ(IPF)/Δ(iPOPAN) was plotted versus $\langle \mathrm{NO} \rangle / \langle \mathrm{NO_2} \rangle$ for individual irradiation steps during a series of experiments, where ⟨NO⟩ represents the mean of the NO concentrations measured before and after each photolysis step (similar for NO_2). A linear plot was obtained, as shown in Fig. S3 in the Supporting Information, with an intercept 3.1 ± 0.3 and a slope of 6.7 ± 0.5. The intercept corresponds to the reciprocal of the branching fraction for attack at the formyl group (32 ± 3)%. The slope is the ratio of rate coefficients k_{35a}/k_{51} for the acyl peroxy radical, divided by the radical yield. The ratio k_{35a}/k_{51} thus obtained (2.1 ± 0.3) is identical to that for PAN (2.1 ± 0.2) [32].

Experiments conducted at 270 K in the presence of NO showed considerably reduced yields of AFAN, 15–18%, compared to 30% at room temperature (see Fig. 5). At the same time, acetone yields increased to 45% (iPOPAN + acetone = 50%). The yield of HCOOH at 270 K was found not to depend strongly on the O_2 concentration in the range 20–400 torr. From experiments on ethyl formate carried out at 270 K in the absence of NO, Orlando and Tyndall found $k_{15}/k_{16} = 1.3 \times 10^{19}$ molecule cm^{-3} [19]. On the basis of these measurements, an O_2 dependence would be expected at this temperature. The lack of a dependence of HCOOH on O_2 suggests that the alpha-ester rearrangement is occurring largely from chemically activated alkoxy radicals. Chemically activated processes are well established for alkoxy radicals produced in the exothermic $ROO^{\bullet}$ + NO reaction [11,13,16].

A few experiments were also conducted in the absence of NO. At both 296 and 270 K, the yields of acetone and AFAN were found to be (20–25)%. In these experiments, alkoxy radicals are produced in roughly thermoneutral $ROO^{\bullet}$ + $ROO^{\bullet}$ reactions and are not subject to chemical activation. While such experiments are difficult to interpret quantitatively, because of the variety of peroxy radical cross reactions involved, it does appear that thermalized $HC(O)OC(CH_3)_2O^{\bullet}$ radicals result in higher yields of AFAN relative to acetone, and in fact all of the acetone can thus be accounted for by abstraction at the formyl group (30%). This is in contrast to the experiments containing NO, where the acetone was distinctly larger than the AFAN, especially

at 270 K. Thus, it is probable that the mechanism of acetone production from $HC(O)OC(CH_3)_2O^\bullet$ involves chemical activation. Further theoretical considerations of the $HC(O)OCH(CH_3)O^\bullet$ and $HC(O)OC(CH_3)_2O^\bullet$ radicals can be found in the section Theoretical Calculations.

tert-Butyl Formate. Reaction of Cl atoms with TBF can occur at two sites, leading to the formation of two peroxy/oxy radicals.

$$Cl + HC(O)OC(CH_3)_3\ (+ O_2) \rightarrow HCl + O_2C(O)OC(CH_3)_3 \quad (25a)$$

$$O_2C(O)OC(CH_3)_3 + NO \rightarrow NO_2 + CO_2 + {}^\bullet OC(CH_3)_3 \quad (55a)$$

$$Cl + HC(O)OC(CH_3)_3\ (+ O_2) \rightarrow HCl + HC(O)OC(CH_3)_2CH_2O_2 \quad (25b)$$

$$HC(O)OC(CH_3)_2CH_2O_2 + NO \rightarrow HC(O)OC(CH_3)_2CH_2O^\bullet + NO_2 \quad (55b)$$

The observed products were acetone, HCHO, CO, CO_2, AFAN and the PAN-type compound tBOPAN, $(CH_3)_3COC(O)O_2NO_2$. Formic acid was only observed with very small yields (<3%), and it was probably not formed in a primary channel. Yields are summarized in Table III, and the pathways involved in the oxidation of TBF are shown in the upper half of Reaction Scheme 1. In the presence of NO, high yields of CO_2 (65–80%) were observed along with acetone (35–45%) and AFAN (7–12%); see Fig. 6. No discernible dependence on the NO concentration was found. The combined yield of CO and HCHO was 45–55%, independent of O_2 concentration. Measurements of HCHO at short reaction times, or at high TBF, showed that the direct yield of HCHO is at least 40%. No methyl nitrite or methyl nitrate was observed in the spectra, showing that the yield of CH_3 radicals is minor.

It is expected that reaction at the formyl site will lead to the production of CO_2 and acetone, or tBOPAN.

$$O_2C(O)OC(CH_3)_3 + NO \rightarrow NO_2 + {}^\bullet OC(O)OC(CH_3)_3 \quad (55a)$$

$${}^\bullet OC(O)OC(CH_3)_3 \rightarrow CO_2 + {}^\bullet OC(CH_3)_3 \quad (56)$$

$${}^\bullet OC(CH_3)_3 \rightarrow CH_3 + CH_3C(O)CH_3 \quad (57)$$

$$O_2C(O)OC(CH_3)_3 + NO_2 \rightarrow (CH_3)_3COC(O)O_2NO_2 \quad (58)$$

However, in chamber experiments, where large amounts of NO and NO_2 are present, the *tert*-butoxy radical will not decompose, but rather react with NO or NO_2.

$${}^\bullet OC(CH_3)_3 + NO \rightarrow (CH_3)_3CONO \quad (59)$$

$${}^\bullet OC(CH_3)_3 + NO_2 \rightarrow (CH_3)_3CONO_2 \quad (60)$$

This explains why CH_3 radicals are not observed, and the acetone yield is lower than that of CO_2. The yields of *tert*-butyl nitrite and nitrate were not linear, as a result of the varying NO/NO_2 ratio in the chamber. The combined yield of *tert*-butyl nitrite, *tert*-butyl nitrate, and tBOPAN was (37 ± 5)%, which is somewhat lower than the branching ratio found earlier for abstraction at the formyl group.

Table III Experimental Conditions and Product Yields for the Reaction of TBF with Cl Atoms in the Presence of NO

			Product Yields (%)						
$P(O_2)$ (torr)	[TBF]o ($\times 10^{14}$)	[NO]o ($\times 10^{14}$)	CO_2	CO_2+ tBOPAN	Acetone	Acetone + tBOPAN	AFAN	PAN + $BuONO_x^a$	CO + HCHO
450	3.5	4.7	65	78	31	44	9	26 (37)	47
40	3.5	5.2	78	91	42	55	8	27 (40)	54
140[b]	2.4	9.8	78	90	43	55	12	26 (33)	55
140[b]	4.8	4.8	70	88	37	53	12	35 (43)	39
140[b]	4.9	9.2	65	86	36	57	9	33 (44)	47
140[b]	2.4	28	72	84	43	55	7	24 (32)	46
10[b]	2.5	9.0	78	85	42	49	9	26 (32)	53
20[c]	3.5	5.6	65	71	46	58	3	23 (34)	36

[a] First entry is for tBOPAN; second includes t-BuONO and t-$BuONO_2$.
[b] Ford expt.
[c] Expt. at 270 K.

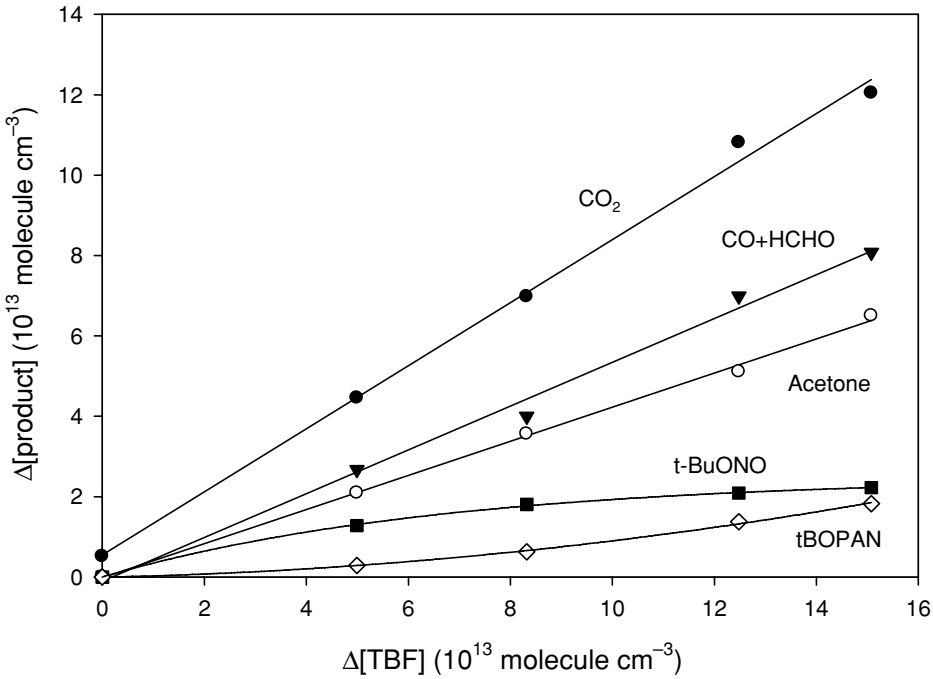

Figure 6 Formation of products from the reaction of Cl atoms with TBF in the presence of NO (5.2×10^{14} molecule cm^{-3}) and 40 torr O_2 (made up to 700 torr with N_2) at 296 K. ●, CO_2; ○, acetone; ▼, CO + HCHO; ■, *tert*-BuONO; ◇, tBOPAN.

Plots of Δ(TBF)/Δ(tBOPAN) versus $\langle NO \rangle / \langle NO_2 \rangle$ were made, as in the IPF experiments, to determine the rate coefficient ratio for reaction of *tert*-butoxy formylperoxy radicals with NO (55a) and NO_2 (58). The intercept corresponded to a yield of 42% for acyl radicals, while the slope gave a ratio of rate coefficients $k_{55a}/k_{58} = 1.7 \pm 0.4$, in good agreement with the isopropyl system.

Abstraction of one of the primary hydrogen atoms leads to the $HC(O)OC(CH_3)_2CH_2O_2$ radical, which reacts with NO to form the alkoxy radical $HC(O)OC(CH_3)_2CH_2O^{\bullet}$. Three possible reactions are likely for this radical: decomposition, reaction with O_2, or isomerization via a six-membered transition state.

$$HC(O)OC(CH_3)_2CH_2O^{\bullet} \rightarrow HCHO + HC(O)OC^{\bullet}(CH_3)_2 \quad (61)$$

$$HC(O)OC(CH_3)_2CH_2O^{\bullet} + O_2 \rightarrow HO_2 + HC(O)OC(CH_3)_2CHO \quad (62)$$

$$HC(O)OC(CH_3)_2CH_2O^{\bullet} \rightarrow {}^{\bullet}C(O)OC(CH_3)_2CH_2OH \quad (63)$$

$${}^{\bullet}C(O)OC(CH_3)_2CH_2OH\ (+O_2, NO) \rightarrow CO_2 + CH_3C(O)CH_3 + HCHO \quad (64)$$

By analogy with oxy radicals derived from substituted ethers [34], and the corresponding radical derived from IPF, reaction with O_2 (62) is not expected to compete with the two other channels. Picquet-Varrault et al. studied the oxidation of a series of acetates and looked for evidence of the production of β-acetoxy carbonyls analogous to the products of reaction (62) [14,15]. Such compounds were identified only when they could be formed from decomposition of a larger oxy radical, not from reaction of a primary radical with O_2.

The radical formed in reaction (61), $HC(O)OC^{\bullet}(CH_3)_2$, is identical to that formed from abstraction at the tertiary site in IPF. However, that radical was shown in the preceding section to give roughly 50% more AFAN than acetone, contrary to what is observed in the case of TBF. A small yield of AFAN is observed ($9 \pm 3\%$), which could come from decomposition of $HC(O)OC(CH_3)_2CH_2O^{\bullet}$. It appears that the primary alkoxy radical $HC(O)OC(CH_3)_2CH_2O^{\bullet}$ predominantly isomerizes via reaction (63), to eventually give CO_2, HCHO, and acetone, and that this accounts for most of the acetone observed in these experiments. The alkoxy carbonyl radicals formed from the isomerization reaction are probably chemically activated and possess enough energy to decompose spontaneously by elimination of CO_2, rather than adding O_2.

$${}^{\bullet}C(O)OC(CH_3)_2CH_2OH \rightarrow CO_2 + {}^{\bullet}C(CH_3)_2CH_2OH \quad (65)$$

This behavior is in contrast to the isopropyl case, where the alkoxy radical formed from the primary methyl groups was found to eliminate HCHO. The reason for this difference is unknown. It is probable that the decomposition and isomerization channels are active to some extent in both molecules (see results of theoretical calculations later); however, the existence of multiple pathways to acetone precludes any more quantitative analysis. Experiments at 270 K and in the absence of NO at 296 K led largely to the same product distribution as described above.

Reactions of IPF and TBF with OH Radicals

In the atmosphere, the oxidation of these esters will be initiated predominantly by reaction with OH radicals, and so a limited number of experiments was performed to investigate the reaction mechanisms with OH. Both methyl and ethyl nitrites were used as photolytic sources of OH.

In the case of IPF, the same set of products was formed as with Cl-initiated oxidation, although quantitative differences were found in the product distribution (see Fig. 7). The observed yields were AFAN (43%), acetone (43%), and HCOOH (15–20%). The higher yield of AFAN is consistent with more abstraction at the tertiary site (55–65%), compared to the chlorine atom reaction. At long reaction times, as the ratio NO_2/NO increased, the yield of iPOPAN approached 20–25%, suggesting that the yield of abstraction at the H—C(O) group is similar to the chlorine experiments. The product yields given above should correspond closely with those found in the atmosphere, where oxidation is largely initiated by OH radicals.

It is expected that OH radicals are produced in the Cl-atom studies following generation of HO_2.

$$HO_2 + NO \rightarrow OH + NO_2 \quad (19)$$

$$OH + IPF \rightarrow \text{product} \quad (66)$$

Simulations of the chemical mechanism using the Acuchem program [37] indicated that for the Cl-atom experiments, up to 30% of the attack on IPF could be from OH radicals, necessitating a revision of the product yields from Cl-atom attack. The preferred values are then: reaction at the formyl group, (30 ± 5)%, reaction at the methyl groups, (20 ± 5)% leading to HCOOH, and reaction at the tertiary carbon, (50 ± 5)% leading to 30% AFAN and (15–20)% acetone. The branching ratios for OH reaction, which are relevant to the atmosphere, remain the same as measured here.

When TBF was oxidized by OH, the yields were essentially identical to the Cl-initiated oxidation, i.e., AFAN <10%, acetone ~40%, acetone + *tert*-BuONO + *tert*-$BuONO_2$ ~ CO_2 ~70%. Hence, the OH-initiated oxidation of TBF also proceeds by roughly

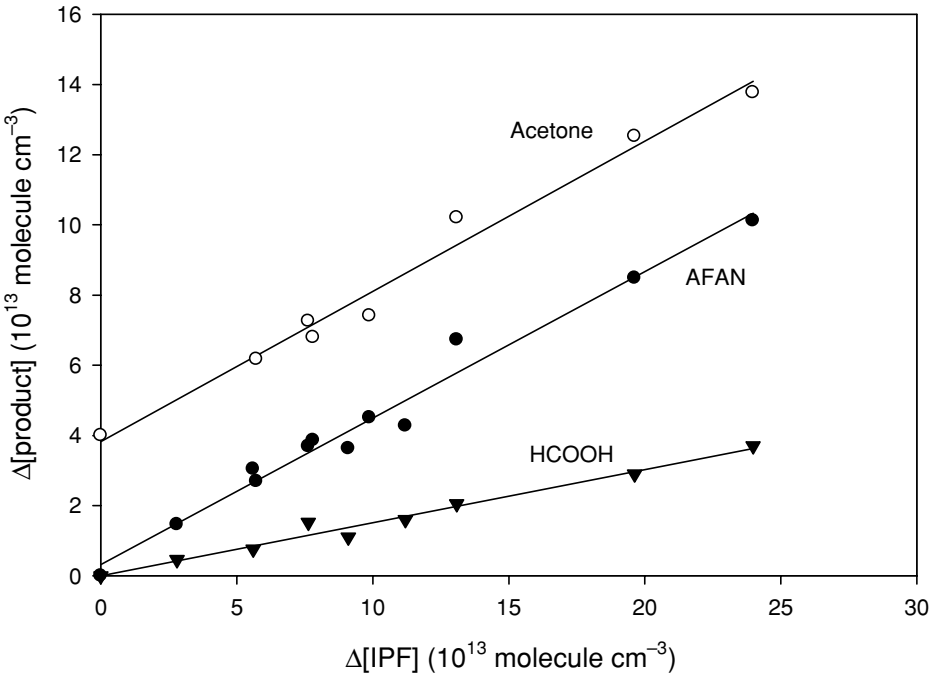

Figure 7 Formation of products from the reaction of OH radicals with IPF in air (140 torr O_2 + 560 torr N_2) at 296 K.

equal abstraction at the formyl and primary sites. At long reaction times, formation of tBOPAN was found, confirming a substantial fraction of attack at the formyl group. The slow rate of reaction of OH with TBF [28,38], and low yields of AFAN, made more quantitative description difficult. In the atmosphere, where *tert*-butoxy radicals decompose rather than react with NO or NO_2, the major product will be acetone with a yield >80%, regardless of the site of attack.

THEORETICAL CALCULATIONS

To interpret the experimental results, quantum chemical calculations were carried out to determine the structures and energies of some of the transition states in the IPF system. The alkyl and alkylperoxy radicals are expected to follow well-documented reactions. However, the behavior of the oxy radicals cannot be predicted easily. Calculations were carried out for the two initially formed oxy radicals, $HC(O)OCH(CH_3)CH_2O^\bullet$ and $HC(O)OC(CH_3)_2O^\bullet$, and for the radical formed by decomposition of the alkoxy radical formed by abstraction at the primary site, $HC(O)OCH(CH_3)O^\bullet$. The reactions considered were decomposition, isomerization, and the alpha-ester rearrangement (for the latter).

Stationary points on the potential energy surfaces for decomposition pathways of the alkoxy radicals were characterized via the CBS-QB3 approach of Petersson and co-workers [39], as implemented in the Gaussian 03 program [40]. Geometries and frequencies, scaled by a standard factor of 0.99 [39], were computed with the B3LYP/6-311G(d,p) level of theory. Next, the energies were derived via coupled cluster (CCSD(T)) theory with approximate extrapolation to the complete basis set limit. For stable molecules, this approach yields atomization energies with a mean absolute deviation of 0.6 kcal mol^{-1} from experiment. Rate constants for unimolecular decomposition at the high-pressure limit were derived via conventional transition state theory [41]. The reaction rate constants should be close to the high-pressure limiting values under the experimental conditions. In the cases of H-atom transfer or elimination pathways, a Wigner tunneling correction was included [42]. This is not expected to be accurate when tunneling is large, but for the present reactions it indicated that at room temperature tunneling increased the reaction rate by only about a factor of 2. The calculated rate constants were well-described by the Arrhenius equation between 200 and 400 K, and the results of the calculations are shown in Table IV.

For the primary $HC(O)OCH(CH_3)CH_2O^\bullet$ radical from IPF, isomerization was calculated to be facile, $\sim 10^9$ s^{-1}, and to dominate over decomposition by loss of HCHO.

$$HC(O)OCH(CH_3)CH_2O^\bullet \rightarrow {}^\bullet C(O)OCH(CH_3)CH_2OH \quad (67)$$

$$HC(O)OCH(CH_3)CH_2O^\bullet \rightarrow HCHO + HC(O)OC^\bullet H(CH_3) \quad (40)$$

The calculated decomposition rate, $\sim 10^6$ s^{-1}, is very similar to those estimated by Aschmann and Atkinson [34] for analogous radicals formed in ether oxidation. The experimental observations presented here suggest that the radical decomposes and that the calculated activation energy for the isomerization may be too low.

For the $HC(O)OC(CH_3)_2O^\bullet$ radical, loss of a methyl group (42) is calculated to be more rapid than the

Table IV Calculated Unimolecular Reaction Rates at the High Pressure Limit for Oxy Radicals

Radical/Reaction	Barrier at 0 K (kcal mol^{-1})	A (s^{-1})	E_a (kcal mol^{-1})	k_{298} (s^{-1})
$HC(O)OCH(CH_3)CH_2O^\bullet$				
HCHO loss	9.4	5.2E13	10.2	1.7E6
Isomerization	4.7	1.1E12	4.2	9.8E8
$HC(O)OC(CH_3)_2O^\bullet$				
CH_3 loss	9.4	1.8E14	10.2	5.6E6
HCO_2 loss	14.3	1.9E13	14.9	220
Isomerization	10.8	2.8e12	10.3	7.7E4
$HC(O)OCH(CH_3)O^\bullet$[a]				
HCO_2 loss	25.5/21.0	5.0E13	26.2/21.7	2.3E-6/5.6E–3
Isomerization	15.8/11.2	3.4E12	15.4/10.8	16/3.8E4
α-ester	11.9/7.3	8.9E12	12.3/7.7	4.6E3/2.1E7
H loss	17.5/12.9	2.2E13	17.6/13.0	2.3/5.7E3
CH_3 loss	13.0/14.4	8.9E13	13.6/15.2	1.3E4/5.8E2

[a]First numbers refer to more stable conformer, A, second numbers to less stable conformer, B.

isomerization channel via a five-membered transition state (44), with computed rate coefficients of $\sim 10^6$ and $\sim 10^5$ s^{-1}, respectively. The difference arises largely because isomerization via the ring is entropically unfavorable and has a pre-exponential factor $\sim 10^2$ times smaller than for C—C bond cleavage.

$$HC(O)OC(CH_3)_2O^\bullet \rightarrow HC(O)OC(O)CH_3 + CH_3 \quad (42)$$

$$HC(O)OC(CH_3)_2O^\bullet \rightarrow {}^\bullet C(O)OC(CH_3)_2OH \rightarrow\rightarrow \text{acetone} \quad (44)$$

Cleavage of the C(O)—O bond was calculated to be much slower, $\sim 10^2$ s^{-1}, as predicted by Aschmann and Atkinson [34] and Good and Francisco [35] for similar species.

$$HC(O)OC(CH_3)_2O^\bullet \rightarrow HC(O)O + CH_3C(O)CH_3 \quad (47)$$

Calculations were also carried out at a lower level of theory B3LYP/6-311G(2df,2p). The barriers for reactions (42), (44), and (47) were calculated to be 11.3, 10.2 and 12.9 kcal mol^{-1}, respectively, in very good agreement with those at the higher level (shown in Table IV). It is reassuring that such good agreement can be obtained with a lower level of theory.

Experimentally, we observed the yield of AFAN from this radical to be approximately three times greater than the yield of acetone. Experiments without NO present showed production of AFAN from this radical to dominate over acetone at both 296 and 270 K. The observations imply that the production of acetone from the tertiary radical is mediated through chemically activated radicals, either by isomerization or from the loss of HC(O)O. This suggests that the barrier for the channel leading to acetone production is smaller than that leading to AFAN, allowing for preferential activation of that channel.

The final radical to be studied, $HC(O)OCH(CH_3)O^\bullet$, is interesting in that it has two relatively stable configurations separated by a few kcal mol^{-1}: one (A) in which the carbonyl oxygen is hydrogen bonded to the hydrogen atom adjacent to the ether linkage, and one (B) in which the oxygen atom bearing the unpaired electron is hydrogen bonded to the formyl H-atom. The calculations show that (A) is the more stable conformer by 4.6 kcal mol^{-1}, with a barrier to interconversion of 7.4 kcal mol^{-1}, which leads at 298 K to a rate of interconversion A→B of 4×10^6 s^{-1} and B→A of 9×10^9 s^{-1}. These rates should be sufficiently rapid that thermal equilibrium is maintained between the conformers. Hence, the overall reaction rate should correspond to a weighted sum of the two conformers. The calculated loss rate of $-CH_3$ radicals (50) is 10^3–10^4 s^{-1} from either conformer. The alpha ester rearrangement (15) is calculated to have rates of 4600 s^{-1} from conformer (A) and 2×10^7 s^{-1} from (B).

$$HC(O)OCH(CH_3)O^\bullet \rightarrow HC(O)OCHO + CH_3 \quad (50)$$

$$HC(O)OCH(CH_3)O^\bullet \rightarrow HC(O)OH + CH_3CO \quad (15)$$

Transition states for these two reaction pathways are shown in Fig. 8, and Fig. 9 shows an Arrhenius plot of all the possible unimolecular pathways from this radical. The experimental evidence [19] shows that the rate coefficient for the alpha-ester rearrangement (15) is of the order 5×10^5 s^{-1}, with a barrier of 8–9 kcal mol^{-1}, intermediate between those calculated for conformers (A) and (B). Raising the energy of conformer (A) relative to both conformer (B) and the transition state by around 2 kcal mol^{-1} would largely take away the discrepancy. No experimental evidence was found for formic anhydride produced in reaction (50), although Picquet-Varrault et al. [15] found evidence for

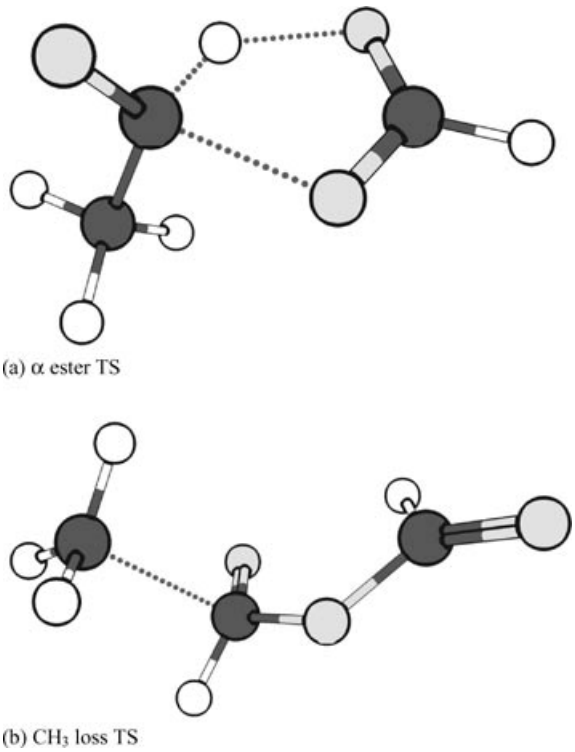

Figure 8 Transition states for the α-ester rearrangement and for loss of a methyl group from the $HC(O)OCH(CH_3)O^\bullet$ radical.

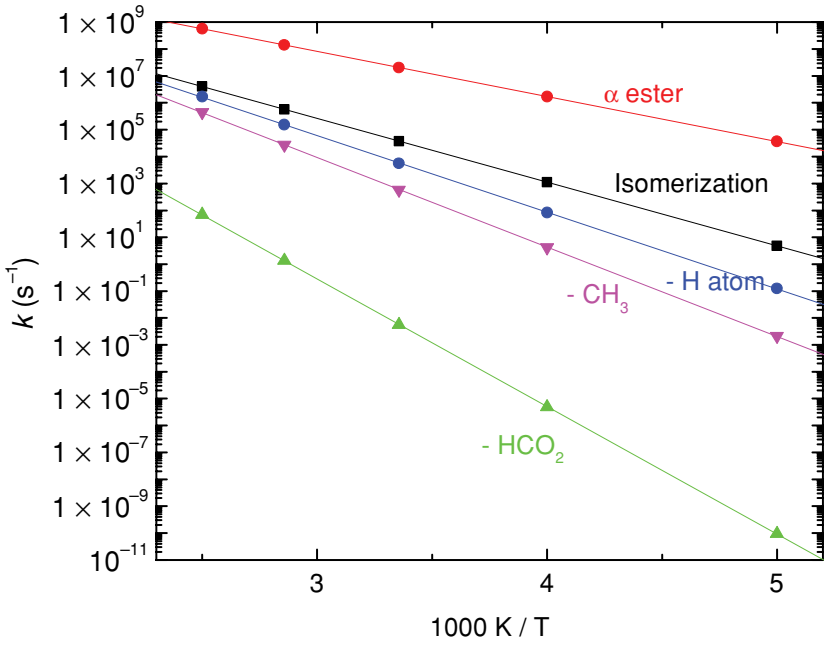

Figure 9 Arrhenius plot showing the rates of the different unimolecular reaction pathways for the $HC(O)OCH(CH_3)O^{\bullet}$ radical. [Color figure can be viewed in the online issue, which is available at www.interscience.wiley.com.]

decomposition of the analogous radical from isobutyl acetate.

The transition state for the alpha-ester rearrangement is difficult to calculate, since it involves the simultaneous breaking of two bonds and shifts of the carbonyl electrons from one oxygen atom to the other [17,18]. However, the present calculations indicate that the decomposition rates are similar in magnitude to those observed and that the decomposition and rearrangement reactions should be competitive, even if the exact ordering of reaction channels is difficult to reproduce. The dynamics of the reactions is undoubtedly complicated by the presence of internal hydrogen bonds in the radicals, which affect both the thermochemistry and the stereochemistry of the reactions.

DISCUSSION

The studies described in the preceding sections show that the major products from the oxidation of IPF in the presence of NO are acetone, AFAN, and formic acid, along with CO, CO_2, and formaldehyde. It is difficult to assign an unambiguous reaction mechanism, since each of the radicals can react by more than one channel, and each product can be formed by more than one pathway. Furthermore, none of the pathways is strongly dependent on the oxygen partial pressure (and in fact any weak O_2 dependences observed are probably a result of changes in the NO/NO_2 ratio). However, significant insight into the mechanism can be gained based on the knowledge of the reaction branching fractions and from the behavior of the product yields as a function of temperature.

Formic acid was observed from the oxidation of IPF for all experiments, regardless of temperature or oxygen partial pressure. While it is expected that its production results from the alpha-ester rearrangement of $HC(O)OCH(CH_3)O^{\bullet}$, it is possible that there exists a further, unidentified channel leading to HCOOH production.

At room temperature, it appears that decomposition of the $HC(O)OC(CH_3)_2O^{\bullet}$ radical results in the formation of AFAN (by methyl elimination), which dominates over acetone formation (probably by isomerization). This can be understood by virtue of the fact that decomposition reactions normally have a large A-factor and large activation barrier, whereas isomerization reactions have both a smaller A-factor and smaller barrier [43]. Furthermore, the experiments without NO present showed roughly equal yields of AFAN and acetone at room temperature. These observations together imply that the production of acetone from the tertiary radical is mediated through chemically activated radicals. Simple bond additivity calculations give an enthalpy of decomposition for $HC(O)OC(CH_3)_2O^{\bullet}$ of 0 ± 2 kcal mol^{-1}, whereas that for $CH_3OC(CH_3)_2O^{\bullet}$ is -5 ± 2 kcal mol^{-1}. Hence the driving force going from ether to ester is stronger than that from ester to anhydride, and as a consequence, the decomposition

reactions do not dominate as much as they do for ethers [34,43].

An interesting aspect of these mechanisms is the production of activated alkoxy radicals from the reaction at the formyl site. Reactions of acyl peroxy radicals with NO are generally quite exothermic (~20 kcal mol^{-1}) and lead to the formation of unstable acyloxy radicals, which decompose very rapidly. The overall exothermicity of the reaction sequence represented by (68) could be as much as 30 kcal mol^{-1} [22].

$$O_2C(O)OC(CH_3)_2R + NO \rightarrow NO_2 + CO_2 + [(CH_3)_2RCO^{\bullet}]^{\ddagger} \quad (68)$$

Although a small barrier is predicted for the decomposition of $ROCO_2$ radicals [35], under conditions of chemical activation their decomposition should be facile. Depending on how the energy is disposed, the resulting isopropoxy or *tert*-butoxy radicals could have sufficient energy to decompose spontaneously (barriers 15.5 and 14.3 kcal mol^{-1}, respectively [43]).

$$[(CH_3)_2RCO^{\bullet}]^{\ddagger} \rightarrow CH_3 + CH_3C(O)R \quad (69)$$

There was some evidence for prompt decomposition of the alkoxy radicals. For example, in experiments where NO was added to the tBOPAN, formation of acetone was observed with a yield of 30% per tBOPAN decomposed. While not totally quantitative, these experiments suggest that as much as one third of the *tert*-butoxy radicals are formed with sufficient energy to decompose before being trapped by NO or NO_2. Normally, chemical activation of alkoxy radicals produced from the reaction of NO with RO_2 radicals is only observed when the barriers to decomposition are relatively low. The requirement for a low barrier limits the effects of chemical activation to substituted

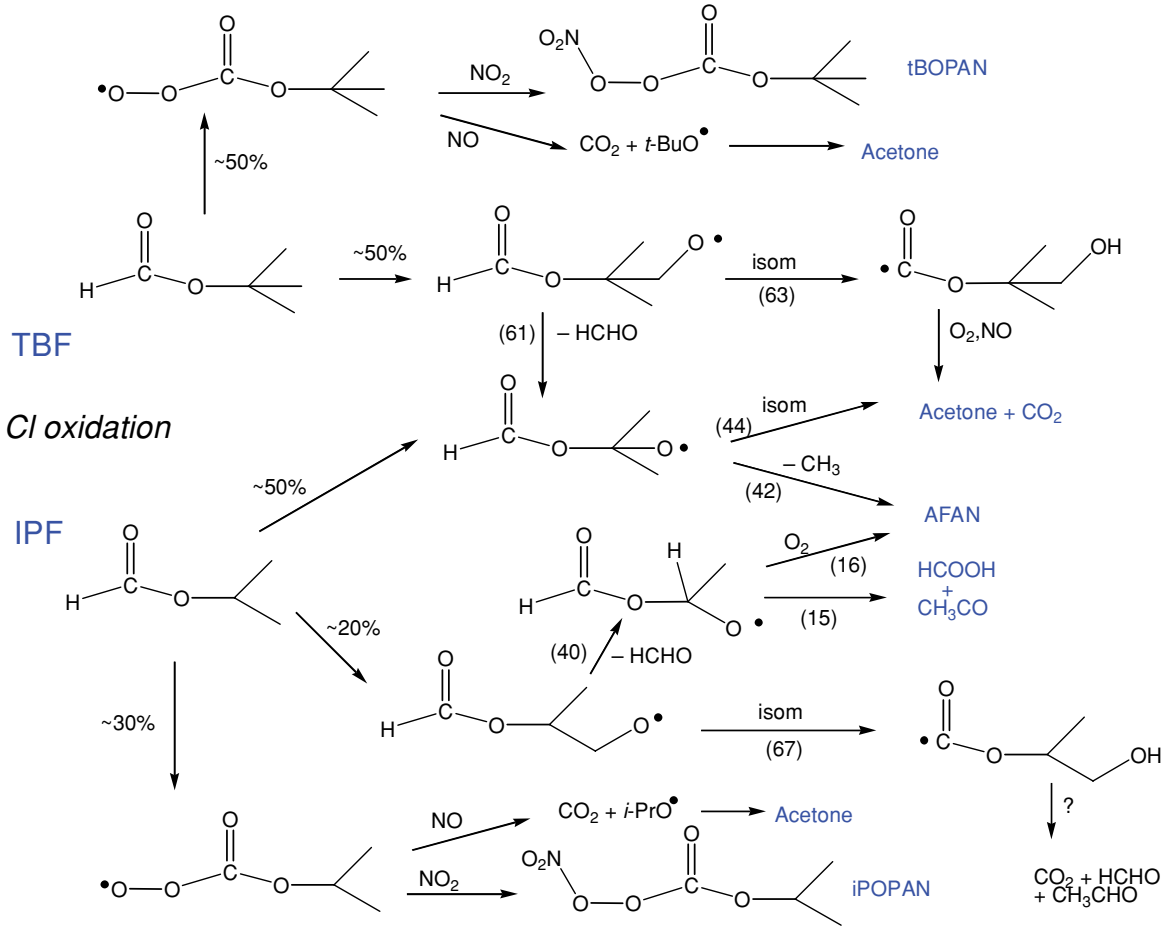

Reaction Scheme 1 Schematic of the oxidation of IPF and TBF, showing common mechanistic features. Reaction numbers correspond to those in text. [Color figure can be viewed in the online issue, which is available at www.interscience.wiley.com.]

radicals (e.g., $CF_3CFHO^{\bullet}$, $HOCH_2CH_2O^{\bullet}$) [43]. The present systems have extra energy available from decomposition of the acyloxy radical, so the energy that is deposited can approach the barriers for the unsubstituted alkoxy radicals $(CH_3)_2CHO^{\bullet}$ and $(CH_3)_3CO^{\bullet}$.

In the case of IPF, no products were observed that could be unequivocally attributed to this activated decomposition process. However, the possibility also exists that highly activated isopropoxy radicals could react with O_2 more rapidly than thermally equilibrated radicals. This would explain the fact that the isopropyl nitrite and nitrate were typically below the detection limit. Some decomposition of hot isopropoxy to $CH_3CHO + CH_3$ radicals cannot be totally ruled out.

Isomerization of alkoxy radicals occurs in both schemes, leading to abstraction of the formyl hydrogen. In the case of $HC(O)OC(CH_3)_2O^{\bullet}$, the isomerization occurs via a five-membered intermediate. Normally this transition state would not be favorable as a result of ring strain, but the weak H—C(O) bond reduces the activation energy and enhances the reaction rate. More theoretical work is clearly needed to understand the role of these strained isomerization reactions.

Overall, the oxidation of isopropyl and *tert*-butyl formates provides a rich chemistry. The mechanisms proposed here, while not unique, provide a description of the chemistry, which is in agreement with our understanding of ester chemistry based on previous studies.

Reaction Scheme 1 summarizes the mechanisms involved in the formation of the observed products, with branching fractions shown for the Cl atom reactions. In the atmosphere, where reaction will proceed by OH attack, it is expected that IPF will form AFAN (40–45%), acetone (40–45%), and formic acid (15–20%). TBF will give a high yield of acetone and CO_2 (80–90%). Depending on the levels of NO and NO_2 present, small amounts of the acylperoxy nitrates may also be formed. Hydrolysis and rain-out of the soluble products should also be considered for a full understanding of the atmospheric fate of these molecules.

SUPPORTING INFORMATION

Figure S1 Plot of the yield of $(CH_3)_2CHOC(O)Cl$ versus consumption of IPF in the absence of O_2. Data are shown for three experiments with Cl_2 in the range $(3–34) \times 10^{14}$ molecule cm^{-3}. The slope (0.30 ± 0.03) gives the yield of abstraction at the formyl hydrogen.

Figure S2 Plot of the yield of CO_2 versus consumption of TBF from three experiments in the absence of O_2. Filled circles: $Cl_2 = 6.4 \times 10^{14}$; open circles: $Cl_2 = 1.3 \times 10^{15}$; triangles: $Cl_2 = 3.2 \times 10^{14}$ molecule cm^{-3}. The slope (0.49 ± 0.05) gives the yield of abstraction by Cl at the formyl hydrogen.

Figure S3 Plot of the reciprocal iPOPAN yield against the mean ratio NO/NO_2 for individual photolysis periods in the reaction of IPF with Cl atoms in the presence of NO.

NCAR is operated by the University Corporation for Atmospheric Research under sponsorship from the National Science Foundation. Computer facilities at UNT were purchased with NSF grant CHE-0342824, and PM is grateful to the R. A. Welch Foundation (Grant B-1174) and the UNT Faculty Research Fund for support. We thank Julia Lee Taylor, Eric Apel, and an anonymous reviewer for their comments on the manuscript.

BIBLIOGRAPHY

1. Legreid, G.; Lööv, J. B.; Staehelin, J.; Hueglin, C.; Hill, M.; Buchmann, B.; Prevot, A. S. H.; Reimann, S. Atmos Environ 2007, 41, 8409–8423.
2. Japar, S. M.; Wallington, T. J.; Richert, J. F. O.; Ball, J. C. Int J Chem Kinet 1990, 22, 1257–1269.
3. Tuazon, E. C.; Carter, W. P. L.; Aschmann, S. M.; Atkinson, R. Int J Chem Kinet 1991, 23, 1003–1015.
4. Smith, D. F.; Kleindienst, T. E.; Hudgens, E. E.; McIver, C. D.; Bufalini, J. J. Int J Chem Kinet 1991, 23, 907–924.
5. Karl, T.; Apel, E.; Hodzic, A.; Riemer, D.; Blake, D.; Wiedinmyer, C. Atmos Chem Phys 2009, 9, 271–285.
6. Arp, H. P. H.; Fenner, K.; Schmidt, T. C. Environ Sci Technol 2005, 39, 3237–3244.
7. Thiault, G.; Thevenet, R.; Mellouki, A.; Le Bras, G. Phys Chem Chem Phys, 2002, 4, 613–619.
8. Zhou, S.; Barnes, I.; Zhu, T.; Bejan, I.; Benter, T. J Phys Chem A, 2006, 110, 7386–7392.
9. Gaffney, J. S.; Marley, N. A. Atmos Environ 2009, 43, 23–36.
10. Tuazon, E. C.; Aschmann, S. M.; Atkinson, R.; Carter, W. P. L. J Phys Chem A 1998, 102, 2316–2321.
11. Christensen, L. K.; Ball, J. C.; Wallington, T. J. J Phys Chem A, 2000, 104, 345–351.
12. Cavalli, F.; Barnes, I.; Becker, K. H.; Wallington, T. J. J Phys Chem A 2000, 104, 11310–11317.
13. Wallington, T. J.; Hurley, M. D.; Maurer, T.; Barnes, I.; Becker, K. H.; Tyndall, G. S.; Orlando, J. J.; Pimentel, A. S.; Bilde, M. J Phys Chem A 2001, 105, 5146–5154.
14. Picquet-Varrault, B.; Doussin, J. F.; Durand-Jolibois, R.; Carlier, P. Phys Chem Chem Phys 2001, 3, 2595–2606.
15. Picquet-Varrault, B.; Doussin, J. F.; Durand-Jolibois, R.; Carlier, P. J Phys Chem A 2002, 106, 2895–2902.
16. Tyndall, G. S.; Pimentel, A. S.; Orlando, J. J. J Phys Chem A, 2004, 108, 6850–6856.
17. Rayez, M. T.; Picquet-Varrault, B.; Caralp, F.; Rayez, J. C. Phys Chem Chem Phys 2002, 4, 5789–5794.
18. Ferenac, M. A.; Davis, A. J.; Holloway, A. S.; Dibble, T. S. J Phys Chem A 2003, 107, 63–72.

19. Orlando, J. J.; Tyndall, G. S. Int J Chem Kinet 2010, 42, 397–413.
20. Shetter, R. E.; Davidson, J. A.; Cantrell, C. A.; Calvert, J. G. Rev Sci Instrum 1987, 58, 1427–1428.
21. Christensen, L. K.; Wallington, T. J.; Guschin, A.; Hurley, M. D. J Phys Chem A 1999, 103, 4202–4208.
22. Atkinson, R.; Baulch, D. L.; Cox, R. A.; Crowley, J. N.; Hampson, R. F.; Hynes, R. G.; Jenkin, M. E.; Rossi, M. J.; Troe, J. Atmos Chem Phys 2006, 6, 3625–4055.
23. Notario, A.; Le Bras, G.; Mellouki, A. J Phys Chem A 1999, 102, 3112–3117.
24. Sellevag, S. R.; Nielsen, C. J. Asian Chem Lett 2003, 7, 15–20.
25. Wallington, T. J.; Hurley, M. D.; Haryanto, A. Chem Phys Lett 2006, 432, 57–61.
26. Bryukov, M. G.; Slagle, I.; Knyazev, V. D. J Phys Chem A 2003, 107, 6565–6573.
27. Stemmler, K.; Mengon, W.; Kerr, J. A. J Chem Soc, Faraday Trans 1997, 93, 2865–2875.
28. Szilágyi, I.; Dóbé, S.; Bérces, T.; Márta, F.; Viskolcz, B. Zeit Phys Chem 2004, 218, 479–492.
29. Gierczak, T.; Rajakumar, B.; Flad, J. E.; Burkholder, J. B. Int J Chem Kinet 2009, 41, 543–553.
30. Rüegge, D.; Fischer, H. Int J Chem Kinet 1986, 18, 145–158.
31. Kirchner, F.; Thüner, L. P.; Barnes, I.; Becker, K. H.; Donner, B.; Zabel, F. Environ Sci Technol 1997, 31, 1801–1804.
32. Sehested, J.; Christensen, L. K.; Møgelberg, T.; Nielsen, O. J.; Wallington, T. J.; Guschin, A.; Orlando, J. J.; Tyndall, G. S. J Phys Chem A 1998, 102, 1779–1789.
33. Allen, G.; Remedios, J. J.; Smith, K. M. Atmos Chem Phys 2005, 5, 3153–3158.
34. Aschmann, S.; Atkinson, R. Int J Chem Kinet 1999, 31, 501–513.
35. Good, D. A.; Francisco, J. S. J Phys Chem A 2000, 104, 1171–1185.
36. Malanca, F. E.; Fraire, J. C.; Argüello, G. A. J Photochem Photobiol A 2009, 204, 75–81.
37. Braun, W.; Herron, J. T.; Kahaner, D. Int J Chem Kinet 1988, 20, 51–62.
38. Le Calvé, S.; Le Bras, G.; Mellouki, A. J Phys Chem A 1997, 101, 5489–5493.
39. Montgomery, J. A., Jr.; Frisch, M. J.; Ochterski, J. W.; Petersson, G. A. J Chem Phys 1999, 110, 2822–2827.
40. Frisch, M. J.; Trucks, G. W.; Schlegel, H. B.; Scuseria, G. E.; Robb, M. A.; Cheeseman, J. R.; Montgomery, J. A., Jr.; Vreven, T.; Kudin, K. N.; Burant, J. C.; Millam, J. M.; Iyengar, S. S.; Tomasi, J.; Barone, V.; Mennucci, B.; Cossi, M.; Scalmani, G.; Rega, N.; Petersson, G. A.; Nakatsuji, H.; Hada, M.; Ehara, M.; Toyota, K.; Fukuda, R.; Hasegawa, J.; Ishida, M.; Nakajima, T.; Honda, Y.; Kitao, O.; Nakai, H.; Klene, M.; Li, X.; Knox, J. E.; Hratchian, H. P.; Cross, J. B.; Adamo, C.; Jaramillo, J.; Gomperts, R.; Stratmann, R. E.; Yazyev, O.; Austin, A. J.; Cammi, R.; Pomelli, C.; Ochterski, J. W.; Ayala, P. Y.; Morokuma, K.; Voth, G. A.; Salvador, P.; Dannenberg, J. J.; Zakrzewski, V. G.; Dapprich, S.; Daniels, A. D.; Strain, M. C.; Farkas, O.; Malick, D. K.; Rabuck, A. D.; Raghavachari, K.; Foresman, J. B.; Ortiz, J. V.; Cui, Q.; Baboul, A. G.; Clifford, S.; Cioslowski, J.; Stefanov, B. B.; Liu, G.; Liashenko, A.; Piskorz, P.; Komaromi, I.; Martin, R. L.; Fox, D. J.; Keith, T.; Al-Laham, M. A.; Peng, C. Y.; Nanayakkara, A.; Challacombe, M.; Gill, P. M. W.; Johnson, B.; Chen, W.; Wong, M. W.; Gonzalez, C.; Pople, J. A. Gaussian 03; revision C.02, Gaussian: Pittsburgh, PA, 2004.
41. Johnston, H. S. Gas Phase Reaction Rate Theory; Ronald: New York, 1966.
42. Bell, R. P. The Tunnel Effect in Chemistry; Chapman and Hall: London, 1980.
43. Orlando, J. J.; Tyndall, G. S.; Wallington, T. J. Chem Rev 2003, 103, 4657–4689.